Epithelial cell proliferation in childhood enteropathies

T C Savidge, A N Shmakov, J A Walker-Smith, A D Phillips

Abstract

***Background/Aim*—The aim of this study was to investigate epithelial cell turnover in childhood enteropathy to establish whether common disease related mechanisms operate. Levels of epithelial cell proliferation were measured in children with food intolerance (cows' milk protein intolerance and coeliac disease), and after infection with *Giardia lamblia*, *Cryptosporidium*, and enteropathogenic *Escherichia coli*.**

***Methods*—Comparative measures of epithelial cell proliferation were performed by recording mitotic activity and MIB-1 immunoreactivity in proximal small intestinal biopsy specimens.**

***Results/Conclusions*—A hyperplastic crypt response was evident in all of the disease states examined and was particularly pronounced in coeliac disease and in infection with enteropathogenic *E coli*, where mitotic and MIB-1 labelling indices were significantly raised above control values. In contrast with coeliac disease, increased crypt cell production rates in enteropathogenic *E coli* infection were also due to an expansion of the crypt proliferation compartment, without a comparable increase in crypt cell numbers. Crypt hyperplasia is therefore a common tissue response to mucosal damage in food allergy and infection, although disease specific mechanisms are evident.**

(*Gut* 1996; **39:** 185–193)

Keywords: intestine, epithelium, enteropathy, food allergy, proliferation.

Academic Department of Paediatric Gastroenterology, Queen Elizabeth Hospital for Children, London
T C Savidge
J A Walker-Smith
A D Phillips

Department of Cellular Physiology, The Babraham Institute, Cambridge
T C Savidge
A N Shmakov

Laboratory of Immunomorphology, Institute of Lymphology, Siberian Branch of the Russian Academy of Medical Sciences, Novosobirsk, Russia
A N Shmakov

Correspondence to:
Dr T Savidge, Department of Cellular Physiology, The Babraham Institute, Cambridge CB2 4AT.

Accepted for publication 31 January 1996

The epithelium of the small intestine is in a constant state of renewal, with one of the highest levels of cell production in the body.[1–3] It is well recognised in this tissue that epithelial cell division is confined to the proliferative zones of the crypts of Lieberkühn.[4] These flask shaped cellular structures possess a highly organised hierarchy of proliferating epithelial cells, which originate from monoclonal pluripotent progenitor stem cells situated within the lower crypt cell positions.[4–6] Migration of epithelial cells from the crypt onto the surface epithelium of the villus occurs in an orderly fashion entailing active proliferation of immature cells, decycling, lineage commitment, and cytodifferentiation, respectively.[6 7]

Regulation of epithelial cell proliferation entails complex interactions[8] between the epithelium and neighbouring heterotypic cells within the lamina propria, for example, pericryptal myofibroblasts, as well as components of the extracellular matrix, such as laminin. Soluble trans-acting factors, for example, epidermal growth factor present either within the intestinal lumen or within the systemic circulation, or both, also exert a regulatory influence on epithelial cell proliferation in vivo.[9–11] Disruption of these growth regulatory systems may lead to uncontrolled proliferation and abnormal cellular differentiation, manifested in its most extreme form as the development of malignancy.[2] The regulation of intestinal proliferation and of other processes, such as apoptosis, therefore depends on carefully orchestrated mechanisms of intercellular communication.[12] This permits a fine control between cell birth and loss in the gut, and provides a system of checks and balances that constitutes a barrier to disease.

In many gastrointestinal diseases the mucosa is damaged and exhibits varying degrees of villous atrophy and crypt hyperplasia – that is, the villous and crypt cell populations change in response to the disease and may achieve a new 'steady state.' In early childhood a thin mucosa has been described in cows' milk sensitive enteropathy,[13] where it was suggested that the crypt cell population does not compensate fully for the loss of villous epithelium. In addition, crypt hypoplasia has been reported in familial enteropathy[14] and in microvillus atrophy,[15] contrasting with the crypt hyperplastic response in coeliac disease.[16–19] This indicates that there are differences in the response of crypt epithelial cells to damage. The aim of this study was therefore to investigate epithelial cell turnover in a wide range of enteropathy associated gastrointestinal diseases in childhood to establish if disease-related differences exist.

Methods

Clinical groups

Intestinal epithelial cell proliferation was carefully examined in proximal small intestinal biopsy specimens from children with food intolerances (cows' milk sensitive enteropathy and coeliac disease) and infection (*giardiasis*, *cryptosporidiosis*, and enteropathogenic *E coli* enteritis).

Patients were categorised into six clinical groups:

(1) Controls (CONT) – 11 children (six female/five male; median (SEM) age 22·8 (3·7), range 4-43 months) with a histologically normal mucosa in whom no gastrointestinal cause could be found for their symptoms.

Figure 1: A-D

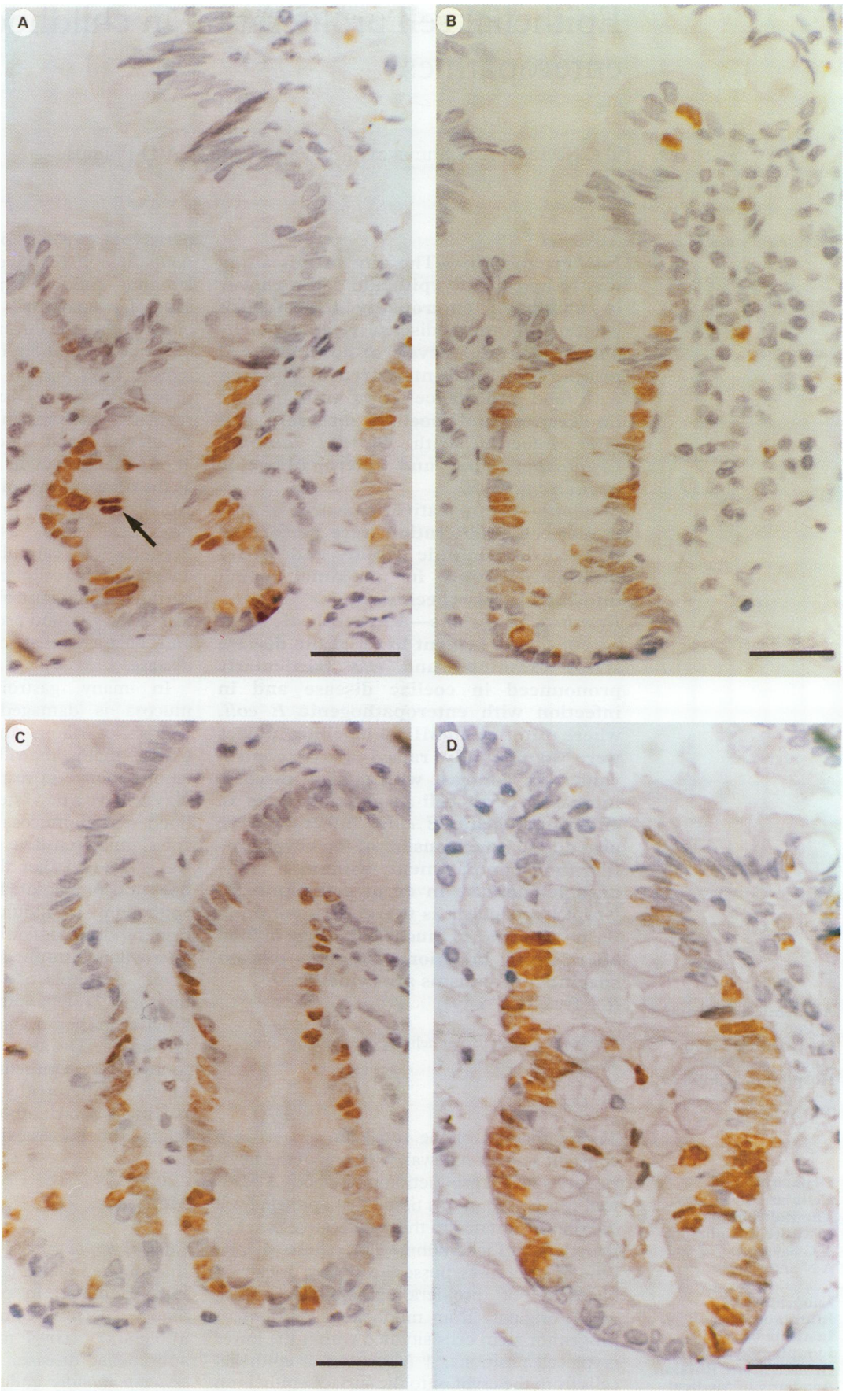

(2) Cows' milk sensitive enteropathy (CMSE) – 14 children (six female/eight male; median age 10·1 (1·60), range 3-22 months), who had an abnormal proximal small intestinal mucosa while receiving cows' milk feeds and who responded clinically to a cows' milk free diet.[20]

(3) Coeliac disease (CD) – 11 children with active CD (six female/five male; median age 25·9 (7·7), range 11-82 months), five of whom were undergoing gluten challenges that confirmed the diagnosis. The rest were undergoing initial investigation and were provisionally diagnosed as coeliac disease on the basis of their severely abnormal biopsy and a clinical

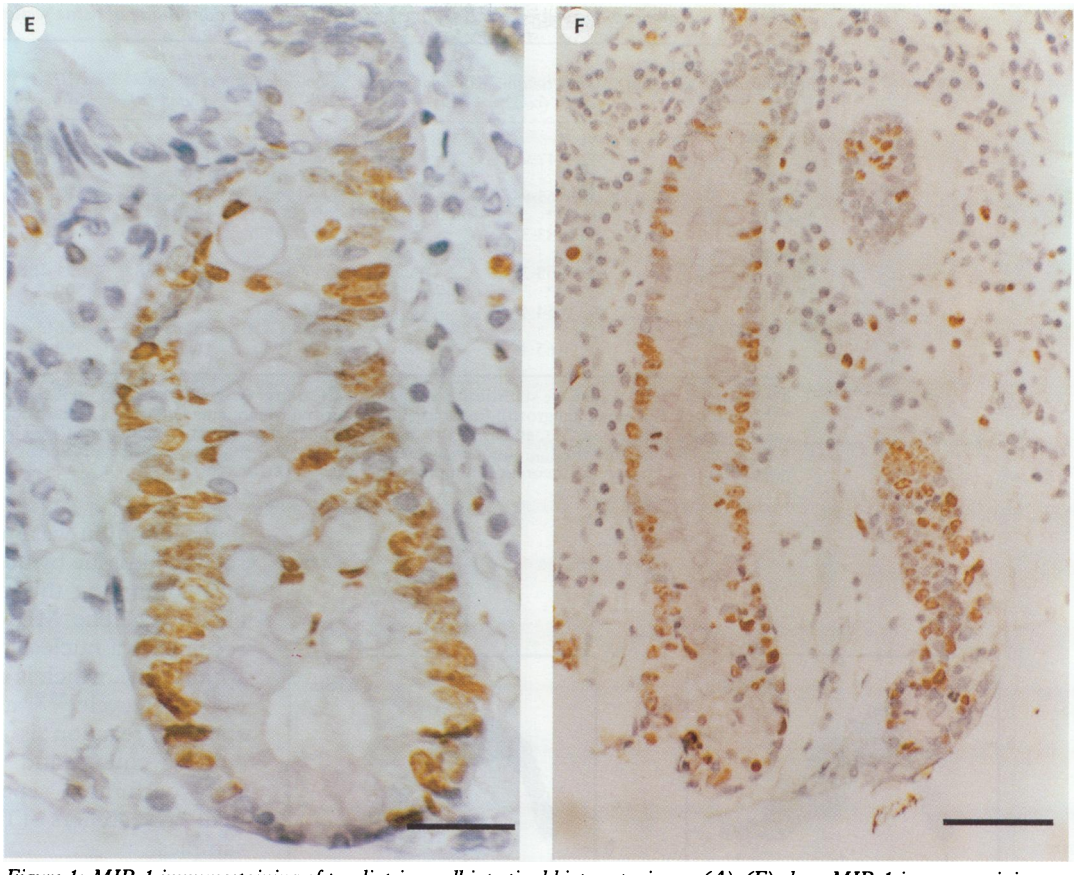

Figure 1: MIB-1 immunostaining of paediatric small intestinal biopsy specimens (A)-(F) show MIB-1 immunostaining (brown DAB reaction product) of intestinal crypts in control, CMSE, CRYPTO, GIARD, EPEC, and CD patients, respectively. The arrow in (A) shows a strongly stained mitotic figure. Scale bars represent 100 μm for (F) and 50 μm for (A)-(E).

response to a gluten free diet. All patients satisfied criteria for the diagnosis of coeliac disease laid down by the European Society of Paediatric Gastroenterology and Nutrition.[21 22]

(4) Giardiasis (GIARD) – Eight children (two female/six male, median age 20·6 (4·0), range 11-46 months).

(5) Cryptosporidiosis (CRYPTO) – Eight children (four female/four male, median age 11·4 (2·3), range 3-22 months).[23]

(6) Enteropathogenic E coli (EPEC) – Five children (three female/two male, median age 8·8 (1·5), range 5-14 months).[24]

In the last three groups *Giardia lamblia, Cryptosporidium*, and enteropathogenic *E coli*, respectively, were identified either in the duodenal juice or in the small intestinal mucosa using light and electron microscopy.

Biopsy procedure

Children were fasted overnight and proximal small intestinal mucosal biopsy specimens were taken under fluoroscopic control from the fourth part of the duodenum or the duodenojejunal flexure using a double port paediatric capsule. All biopsies were performed as part of each child's routine investigations with fully informed consent. Biopsy material was removed from the capsule, orientated on black card, immersed in ice cold NaCl (0·9% w/v), and fixed in 10% phosphate buffered formal saline (pH 7·2) for no more than 12 hours. Tissue was then processed for paraffin wax histology using conventional methods and serial sections (5 μm thick) were cut and stained with haematoxylin and eosin.

TABLE 1 *Summary of kinetic data calculated from analysis of mitotic figures in tissue sections*

	Patients per group (n)	*Crypt column length (cells)*	*Crypt circumference (cells)*	*Total crypt cell population (cells)*	*Mitoses/crypt column (n)*	*I_m corrected (%)*	*GF_{theor} (%) [cells]*	*CCPR (cells/crypt/h)*	*EMR (cell pos/h)*
CONT	11	32·8	22·5	738	0·93	0·97	70	5·6	0·25
		29·1-36·8		654-828	0·71-1·19	0·88-1·34	[496]	4·3-7·2	0·19-0·32
CMSE	14	42·3***	25·3	1069*	1·21**	1·11^{NS}	65	8·0**	0·32**
		33·6-49·5		850-1252	0·78-1·97	0·93-1·75	[609]	5·3-13·4	0·21-0·53
CD	11	73·1***	35·0	2559*	2·21***	1·37**	60	21·0***	0·60***
		60·8-81·1		2128-2839	1·83-3·34	1·19-1·85	[1262]	17·3-31·5	0·50-0·90
EPEC	5	53·5*	27·6	1477*	2·03**	1·60**	68	15·2**	0·55**
		45·1-62·1		1245-1714	1·37-2·80	1·21-1·83	[842]	10·2-21·0	0·37-0·76
GIARD	8	46·9**	28·0	1312**	1·16*	0·98^{NS}	71	8·7**	0·31**
		44·2-62·6		1238-1753	0·93-1·93	0·70-1·17	[949]	7·0-14·6	0·25-0·52
CRYPTO	8	49·9**	28·0	1398**	1·19^{NS}	0·95^{NS}	65	9·1**	0·33^{NS}
		39·8-64·1		1114-1795	0·65-1·91	0·57-1·55	[863]	5·0-14·3	0·18-0·51

Median (and range) values are statistically compared with control (CONT) data (NS=not significant, *=≤0·05, **=≤0·01, ***=≤0·001). Theoretical growth fractions (GF_{theor}) calculated from the I_m frequency distributions curves[17] (Fig 2) are expressed as a percentage of the total crypt cell population (%), and as the theoretical number of proliferating cells/crypt ([]).

TABLE II *Summary of kinetic data calculated from MIB-1 immunostaining of tissue sections*

Clinical group	Patients per group (n)	Crypt column length (cells)	Crypt circumference (cells)	Total crypt cell population (cells)	MIB-1+ cells/crypt column (n)	MIB-1+ cells/crypt (n)	I_{MIB-1} GF_{exp} (%) [cells]	GF_{theor} (%) [cells]
CONT	7	34·7	23·5	815	13·7	322	34·7	81
		32·7-47·9		768-1126	9·9-18·0	232-424	[283]	[660]
CMSE	6	47·7*	27·5	1312**	17·8^{NS}	488*	43·3^{NS}	73
		36·1-63·8		993-1755	11·4-28·0	313-770	[568]	[958]
CD	6	74·9**	36·0	2697**	40·0**	1441**	51·0**	74
		56·8-83·3		2045-2999	28·7-49·4	1033-1778	[1375]	[1996]
EPEC	3	59·0*	29·6	1746*	30·7*	910*	52·1*	84
		41·1-65·3		1217-1933	20·1-46·8	594-1384	[912]	[1467]
GIARD	5	52·8**	28·7	1515**	17·4*	500**	32·0^{NS}	73
		48·0-54·4		1378-1561	14·9-27·4	428-785	[485]	[1106]
CRYPTO	4	55·4*	29·6	1638*	25·6*	756**	41·5^{NS}	71
		44·5-65·4		1317-1936	16·7-32·1	494-951	[680]	[1163]

Median (and range) values are statistically compared with control (CONT) data (NS=not significant, *=≤0·05, **=≤0·01, ***=≤0·001). Experimental growth fractions (GF_{exp}) derived from median crypt I_{MIB-1} values, are expressed as a percentage of the total crypt cell population (%), and as the theoretical number of proliferating cells/crypt ([]). Theoretical growth fractions (GF_{theor}) calculated from the I_{MIB-1} frequency distributions curves[17] (Fig 2), are also expressed as a percentage of the total crypt cell population (%), and as the theoretical number of proliferating cells/crypt ([]).

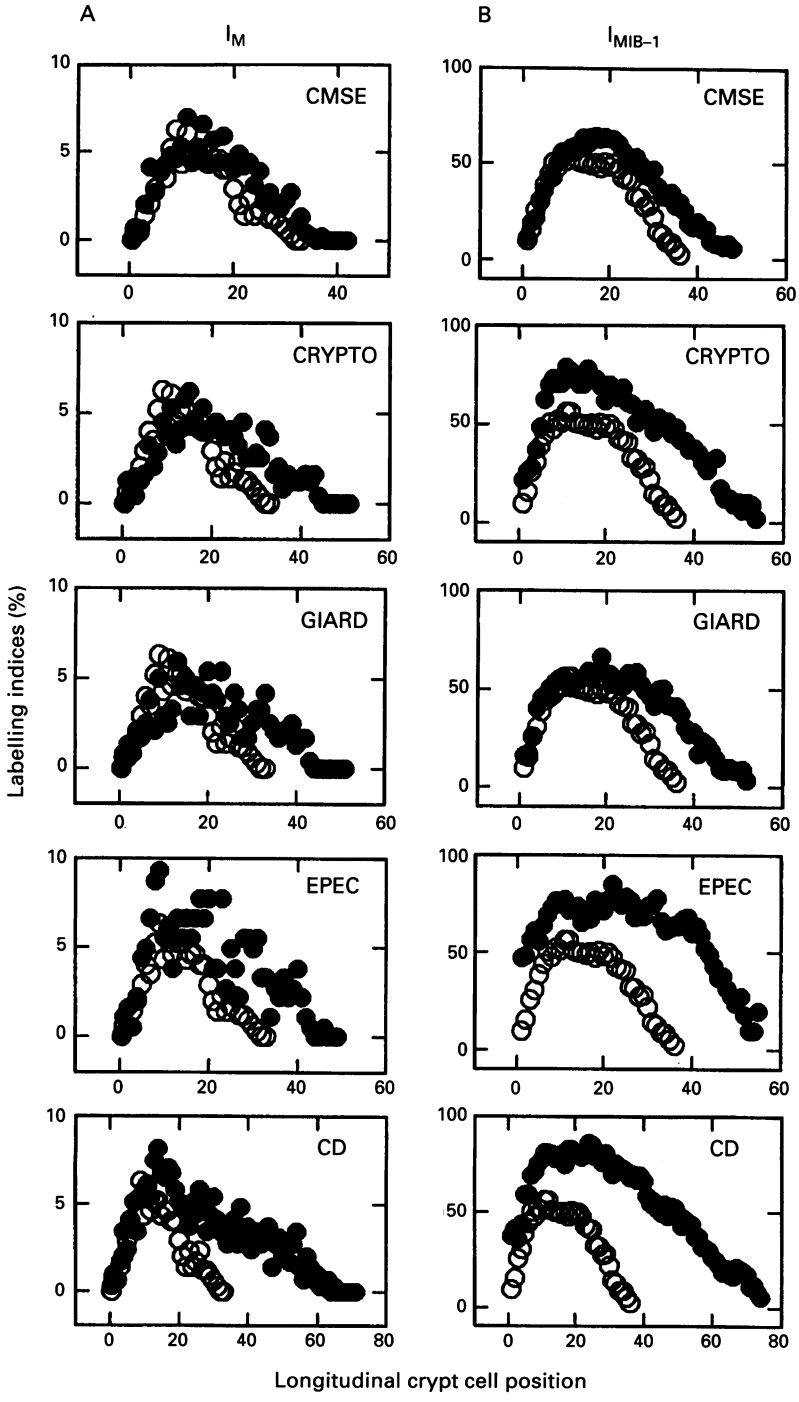

Proliferation was measured in histologically sectioned tissue by quantifying mitotic activity and comparing this to MIB-1 immunohistochemistry. The MIB-1 monoclonal antibody recognises a nuclear non-histone protein (Ki-67 antigen), which is associated with all phases of the cell cycle,[25 26] although the most intense staining reaction is seen in mitotic cells.[27] Mitotic counts and MIB-1 labelling indices were performed separately by two independent researchers (TS and AS) on blind samples.

Mitotic indices

The mitotic index was calculated using a modification of the technique described by Wright *et al.*[17] This method records mitotic figures in haematoxylin and eosin stained longitudinal sections of proximal small intestinal crypts. The number and position of interphase and mitotic nuclei were recorded from 30 well oriented crypts where Paneth cells, a crypt lumen, and a crypt-villous junction were clearly evident.

MIB-1 immunohistochemistry

Paraffin wax sections (5 μm thick) were dewaxed in xylene and rehydrated through graded levels of alcohol. Endogenous peroxidase was blocked in 0·3% hydrogen peroxide for 15 minutes. Sections were then immersed in 10 mM sodium citrate buffer (pH 6·0) and microwaved for a total of 25 minutes (98·6°C) at 600W. After cooling, slides were incubated at room temperature with 1% ovalbumin for 10 minutes and then overnight at 4°C with the MIB-1 monoclonal antibody (1:50 dilution; a generous gift from the Binding Site, Birmingham, UK). Slides were washed (three times) in TRIS buffered saline (TBS, pH 7·4) and incubated with sheep antimouse biotinylated second antibody (1:50 dilution;

Figure 2: Longitudinal crypt distribution of mitotic and MIB-1+ epithelial cells in control and disease patients. A direct comparison of the frequency distribution of (A) mitotic (I_M) and (B) MIB-1 (I_{MIB-1}) labelling indices at each crypt cell position is shown for control (○) and disease (●) groups, respectively. In each case, crypts have been normalised to account for length variations affecting the distribution of proliferating epithelial cells.

Amersham International, Little Chalfont, Buckinghamshire, UK) for one hour, at room temperature. After washing in TBS (three times), slides were incubated with streptavidin-biotinylated horseradish peroxidase complex (diluted 1:100; Amersham) for one hour, at room temperature. Slides were then washed with TBS (three times) and incubated with diaminobenzidine (DAB; Sigma, Poole, Dorset, UK) in the dark for 10 minutes, at room temperature. Sections were finally counterstained with 1% haematoxylin and mounted in Ralmount (Merk Ltd, Poole, Dorset, UK). The number and position of labelled and unlabelled cells were recorded from 30 well oriented crypts as described for counting cells in mitosis.

Analysis of proliferation

Mitotic and MIB-1 labelled cells were recorded into a specialised crypt analysis program,[28] which was developed and kindly made available to us by Professor C S Potten and Dr S A Roberts (Epithelial Cell Biology Group, Paterson Institute for Cancer Research, Christie Hospital, Manchester, UK). Using this program on a digital micro-vax system, crypts were normalised to account for crypt length variations affecting the distribution of mitotic and MIB-1$^+$ epithelial cells. In addition, the program was used to (a) plot mitotic and MIB-1 labelling frequency distribution curves along the longitudinal crypt axis, and (b) to calculate crypt MIB-1 labelling indices (I_{MIB-1}), mitotic indices (I_m), and growth fractions for the respective clinical groups.

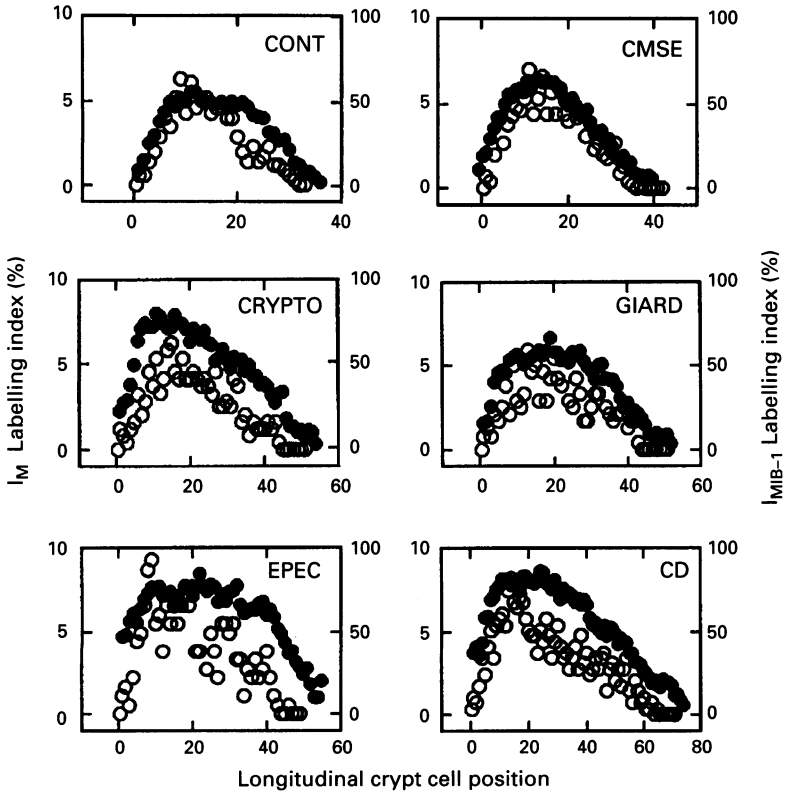

Figure 3: Comparison of the frequency distribution of mitotic and MIB-1$^+$ crypt cells in individual clinical groups. The left and right hand vertical axes (abscissa) represent I_m (○) and I_{MIB-1} (●) labelling indices, respectively. In each case, crypts have been normalised to account for length variations affecting the distribution of proliferating epithelial cells.

The total crypt cell population (TCCP) for each clinical group was calculated by multiplying the average crypt length by the circumference (column count). Tissue was not readily available for measuring column counts (as this entails tangential sectioning of blocks), and these values were obtained from previously published data on childhood gastrointestinal diseases.[17 19] In all cases we assumed there to be a linear correlation between crypt length and circumference, thereby providing values for TCCP that are proportional to the crypt length. In a separate study we showed that these calculated values for TCCP are in a close agreement with data obtained from total crypt cell counts measured using confocal microscopy.[29]

Statistics

Statistical analyses were performed using MINITAB (Minitab Inc, State College, PA-16801-2756, USA) and STATGRAPHICS (Statistical Graphics Corporation, Rockville, Maryland 20852, USA) statistical software. Deviations from the null-hypothesis were tested using the non-parametric Mann-Whitney U test for ranks and analysis of variance (ANOVA); *,**:$p<0.05$, 0.001, respectively; NS, no significant difference.

Results

Histological features

Inspection of haematoxylin and eosin stained sections from each group confirmed previously described histological findings for the respective enteric diseases.[30] The most abnormal samples, as compared with histologically normal controls, were seen in CD where there was clear evidence of hyperplastic crypts and severe villous atrophy. The lamina propria possessed a heavy cellular infiltrate, which included neutrophils. The severity of these lesions was less pronounced in the other disease groups, although occasionally pronounced villous atrophy with epithelial shedding was evident in EPEC, GIARD, and CRYPTO. The least abnormal mucosa was consistently seen in CMSE where there was evidence of mild villous atrophy, crypt hyperplasia, and a less pronounced leucocytic infiltrate. In all of the clinical groups examined, there was a consistent MIB-1 immunostaining pattern and labelling intensity within the crypts, demonstrating the proliferating epithelial cell population (Fig 1A-F). The MIB-1 monoclonal antibody recognised epitopes preferentially situated within the nucleoli and nuclear membrane, confining the DAB reaction product to the nucleus.

Distribution of mitotic and MIB-1$^+$ epithelial cells

Mitotic and MIB-1$^+$ epithelial cells were compartmentalised within the intestinal crypts in all biopsy material examined. Median crypt

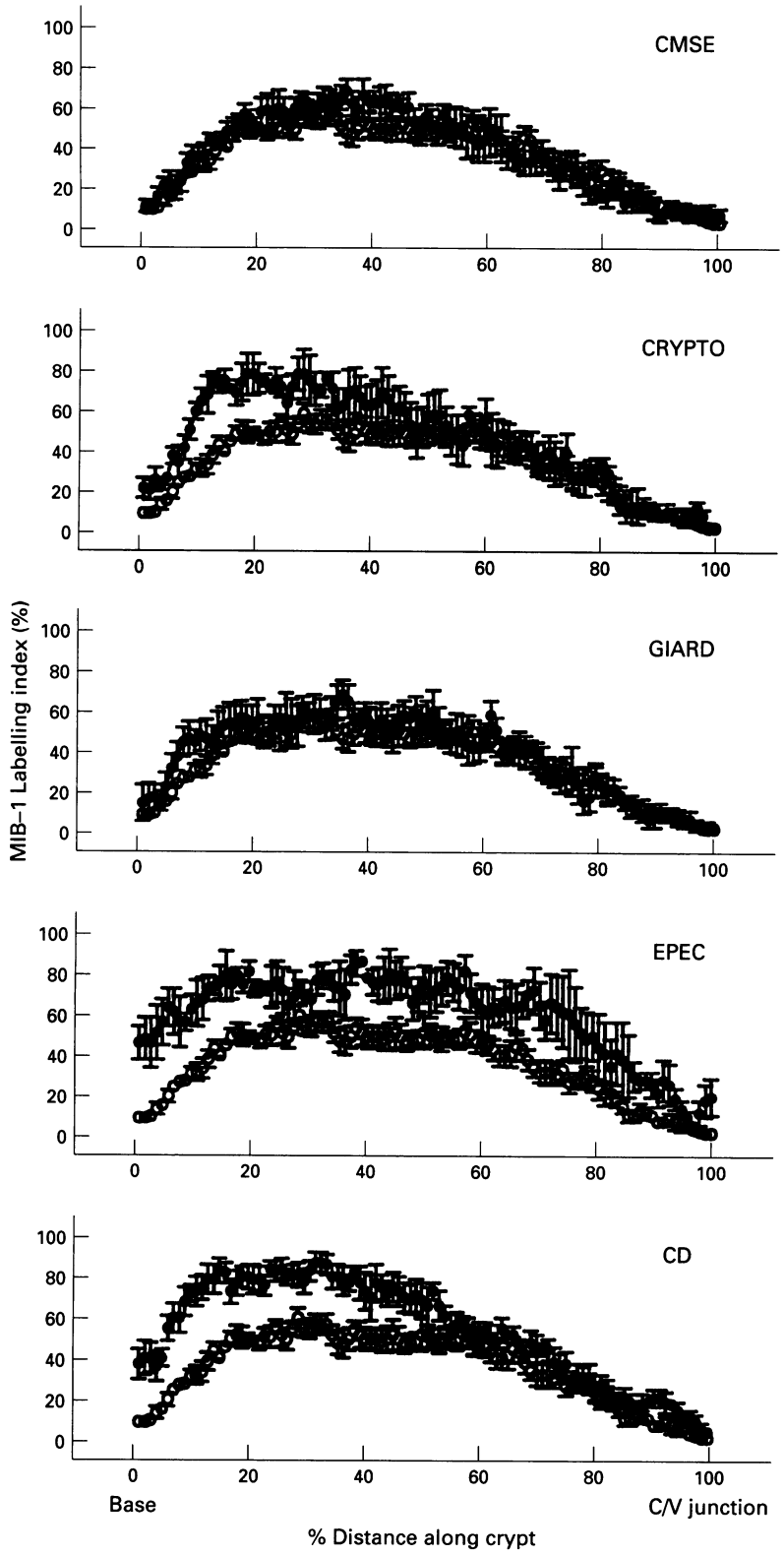

Figure 4: MIB-1 labelling index distribution curves for control (○) and disease (●) groups plotted onto a standardised longitudinal crypt axis. The crypt base and crypt-villous junction have been designated as 0% and 100% of the distance along the crypt, respectively. Vertical error bars show 95% confidence intervals.

dimensions for each of the six clinical groups investigated are summarised in Tables I and II, which also list values for the number of mitoses and MIB-1$^+$ epithelial cells recorded per crypt column. Figures 2 and 3 show the comparison of the frequency distribution curves for mitotic activity (I_m; derived from direct examination of haematoxylin and eosin stained sections), and MIB-1$^+$ labelling (I_{MIB-1}; derived from immunohistochemical staining for the Ki-67 antigen). In all cases, values have been adjusted to median crypt group lengths to avoid individual variation in crypt size influencing the distribution pattern.[31]

Figure 2 shows the control group distribution pattern compared with each disease group in turn. Figure 3 directly compares results for each clinical group, obtained by the two different methods. A common distribution for proliferating cells is clearly shown in the different groups, with most cell division occurring within the lower two thirds of the crypt, and a subsequent linear decline towards the crypt-villous junction (Fig 2). Figures 2 and 3 also show that MIB-1 staining, rather than the direct observation of mitotic figures, gives greater separation between the profiles of disease groups and controls. To analyse this finding more closely, I_{MIB-1} distribution curves were plotted onto a standardised crypt axis (Fig 4). This procedure has been described previously[28] and entails designating cell position one and the crypt-villous junction as 0 and 100% of the crypt length, respectively. When comparing controls with disease groups, it is evident that the higher median crypt I_{MIB-1} in the different enteropathies is caused by a local increase in the number of cycling cells specifically within the proliferation compartment – that is, within the lower two thirds of the crypt. The notable exception being the EPEC group where a raised I_{MIB-1} was recorded throughout the crypt. Similar, although less pronounced, features were also found when comparing standardised control and disease I_m distribution curves (data not shown).

Crypt growth fraction

The crypt growth fraction (GF) was defined as the percentage of epithelial cells that were actively proliferating. This was obtained from (a) experimental values recording the percentage of MIB-1$^+$ cells per crypt column (GF_{exp}), and (b) by calculating theoretical (GF_{theor}) values from the I_m and I_{MIB-1} distribution curves, as has been described previously.[2 17 32] In the last case, this was achieved by extrapolating the 'half mid-way point' or I_m/I_{MIB-1} $max_{50\%}$ values to the x axis, which displays the longitudinal crypt cell position. This position was then used to define theoretical crypt proliferation and maturation compartments, respectively. Experimental and calculated growth fractions were finally expressed as a percentage of the total crypt cell population (Tables I and II; Fig 5). It is clear from these results that experimentally derived values for the growth fraction were consistently smaller (an average of 56% less; Fig 5B) than calculated values, which define the theoretical crypt proliferation compartment.

Epithelial cell migration (EMR) and crypt cell production (CCPR) rates

A geometrical correction factor of 0·27 was applied to all mitotic index data, which was subsequently used to calculate EMR and CCPR using conventional methods.[2] We have

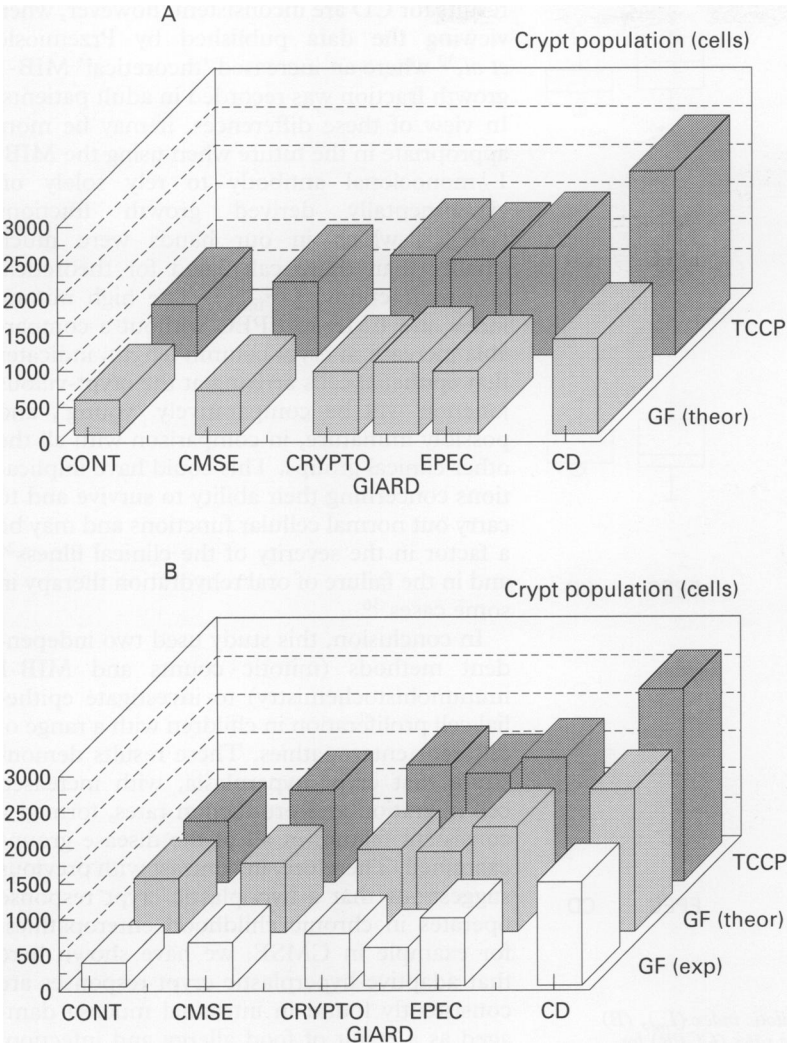

Figure 5: Experimental and theoretical crypt growth fractions. (A) calculated mitotic growth fractions (GF_{theor}) shown as a percentage of the total crypt cell population (TCCP). (B) experimental (GF_{exp}) and calculated (GF_{theor}) MIB-1 growth fractions shown as a percentage of the total crypt cell population (TCCP). Clinical groups have been ranked to show statistical differences between disease groups – that is, the number of proliferating epithelial cells in CRYPTO, GIARD, and EPEC (although not significantly different from each other) are smaller and larger than for CD and CMSE, respectively.

demonstrated previously using confocal microscopical analysis of crypt cell proliferation,[29] that this constant provides a more accurate indicator of CCPR in normal and disease biopsy specimens than using conventional geometrical corrections factors based on the Tannock's principle.[33] Group values for EMR and CCPR are shown in Table I and Fig 6. All disease groups displayed a significant crypt hyperplasia, with an increased crypt cell population and CCPR when compared with controls. However, the extent of this hyperplasia varied significantly between the different disease groups. Analysis of variance demonstrated that the increase in crypt size, both in terms of crypt column length and total crypt cell population, was greater in CD (p=0·002-0·0003) than in EPEC, GIARD, and CRYPTO (which were not different from each other), and all were greater than CMSE (p=0·002-0·00003; Fig 5). On the other hand, when calculating CCPR it was found that EPEC had a higher crypt cell production rate (p=0·01-0·003) than GIARD, CRYPTO, and CMSE (which were not different from each other), although this was still smaller than values calculated for CD (p=0·03-0·0003; Fig 6). This relative increase in CCPR in EPEC was due to a significantly raised crypt I_m when compared with GIARD, CRYPTO, and CMSE (p=0·02-0·0004; which did not differ from controls). A similar observation was seen for the EMR – that is, the epithelial cell migration rate that is calculated from the number of mitoses per crypt column (Table I and Fig 6).

Discussion

This study has investigated intestinal epithelial cell proliferation in proximal small intestinal biopsy specimens from children with a wide range of enteropathies. The aetiology of the enteric diseases included intolerance to cows' milk protein and gluten, and infection – *giardiasis, cryptosporidiosis*, and enteropathogenic *E coli* enteritis. It is clear that crypt hyperplasia occurred in all of the disease groups. This was most apparent in CD where crypts were 2·2-fold longer and possessed 3·5-fold more cells than in controls. The least hyperplastic crypts were recorded in CMSE which were 1·3-fold longer and harboured 1·4-fold more cells than in controls. Although an increased number of mitoses and MIB-1 labelled epithelial cells were recorded in all of the disease groups, the I_m and I_{MIB-1} distribution curves essentially followed a similar pattern, with the highest levels of proliferation occurring in the lower to middle portion of the crypt. However, the significant crypt elongation in disease compared with histologically normal biopsy specimens resulted in mitoses and MIB-1^+ cells being detected in higher cell positions.

On the whole, there was a good correlation between the frequency distribution of mitotic and MIB-1^+ cells within individual groups. This was especially apparent in controls and CMSE, although slight differences were evident in the other disease groups and were particularly noticeable in CD and EPEC. Firstly, the I_{MIB-1} distribution curves showed a more uniform distribution throughout the crypt. This is also demonstrated when regarding the theoretical growth fractions that were calculated from I_{MIB-1} and I_m $max_{50\%}$ values. The proliferation compartment was consistently 10% smaller in the second group, indicating that this theoretical cut off position was situated lower down within the crypt. The inherent problems of obtaining accurate I_m crypt distribution data from two dimensional histological sections were considered recently in a confocal microscopical analysis of mitotic activity within intact micro-dissected crypts from paediatric patients.[29] By avoiding such limitations using confocal microscopy, we demonstrated 'corrected' I_m distribution patterns to be very similar to the MIB-1 frequency distribution curves presented in this work.

Secondly, in groups with a severely abnormal mucosa, for example CD and EPEC, high MIB-1 labelling indices were recorded in regions where little or no mitotic activity could be detected – that is, at the crypt base and

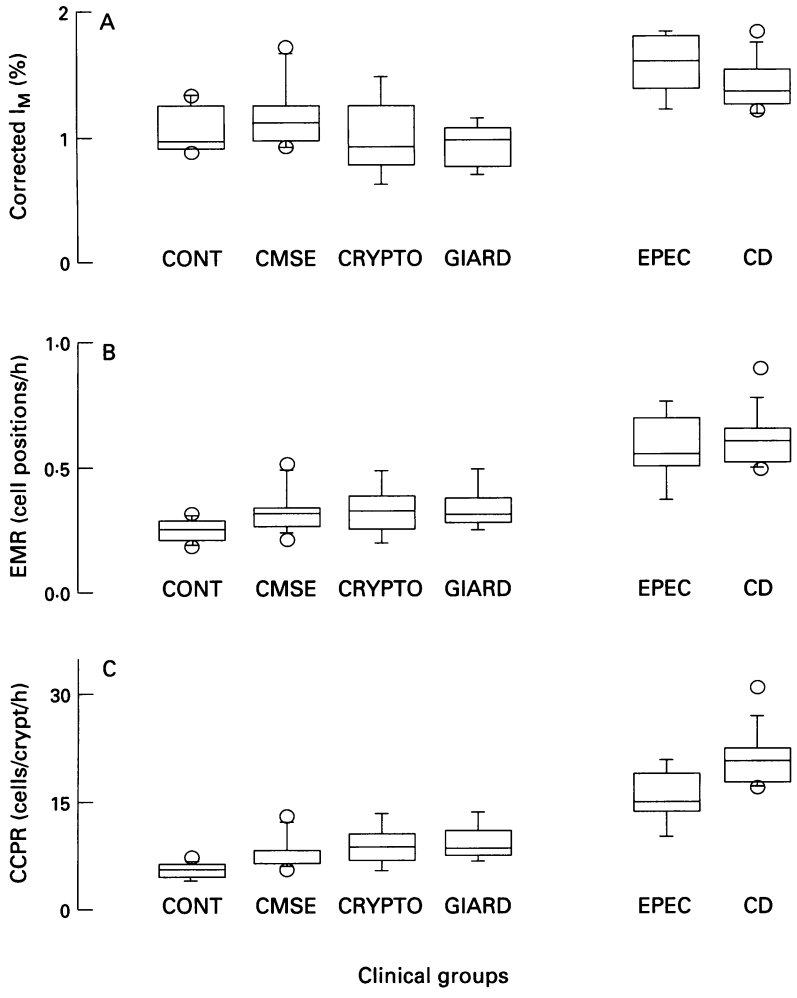

Figure 6: Box and whisker plots showing (A) corrected crypt mitotic index (I_m), (B) epithelial migration rates (EMR), and (C) crypt cell production rates (CCPR) for individual clinical groups, which have been ranked to show statistical differences between disease groups.

towards the crypt-villous junction. In a separate study using human fetal intestine xenografted into severe-combined immunodeficient mice, we have shown similar discrepancies between MIB-1 and tritiated thymidine incorporation in damaged and regenerating human gastrointestinal epithelium.[34] Therefore, although a close correlation between MIB-1 and mitotic activity may be demonstrated in histologically normal intestine, caution still needs to be exercised when using this antibody to investigate severely abnormal tissue. This point has been made previously in a study that demonstrated that the Ki-67 monoclonal antibody consistently overestimated the growth fraction in xenografted human tumours.[35]

The hyperplastic crypt response differed in the various disease groups. In CMSE, CRYPTO, and GIARD the increased EMR and CCPR could be accounted for by a crypt expansion alone, as there was not a significant increase in either I_m or I_{MIB-1}. In contrast, in CD and EPEC higher mitotic and MIB-1 labelling indices were recorded, indicating a possible shortening of the cell cycle duration. This was particularly apparent in EPEC, which possessed high labelling indices throughout an expanded crypt proliferation compartment, without an equivalent increase in the total crypt cell population, as is seen in CD. These results for CD are inconsistent, however, when viewing the data published by Przemioslo *et al*,[32] where an increased 'theoretical' MIB-1 growth fraction was recorded in adult patients. In view of these differences, it may be more appropriate in the future when using the MIB-1 monoclonal antibody to rely solely on experimentally derived growth fractions (GF_{exp}), which in our hands were much smaller than those calculated for theoretical growth fractions (GF_{theor}). The high mitotic index and EMR in EPEC without a comparable increase in crypt column length, indicates that epithelial cells arriving at the crypt-villous junction will be comparatively 'young', and possibly immature, in comparison with all the other clinical groups. This could have implications concerning their ability to survive and to carry out normal cellular functions and may be a factor in the severity of the clinical illness[24] and in the failure of oral rehydration therapy in some cases.[36]

In conclusion, this study used two independent methods (mitotic counts and MIB-1 immunohistochemistry) to investigate epithelial cell proliferation in children with a range of different enteropathies. These results demonstrate that crypt hyperplasia, with increased cell migration and production rates, formed a consistent feature in all of the disease groups examined. Therefore, in contrast with previous suggestions that a hypoplastic crypt response operates in chronic childhood enteropathies, for example in CMSE, we have shown here that adaptive hyperplastic crypt responses are consistently found in intestinal mucosa damaged as a result of food allergy and infection.

The authors wish to thank Professor C S Potten and Drs S A Roberts and D Brown for helpful comments and the Histopathology Department, The Hospital for Sick Children, Great Ormond Street, for technical assistance. This work was supported by the Queen Elizabeth Hospital for Children Research Appeal Trust, The Royal Society, and the BBSRC.

1 Leblond CP. Time dimension in cell biology. A radioautographic survey of the dynamic features of cells, cell components, and extracellular matrix. *Protoplasma* 1991; **160:** 5–38.
2 Wright NA, Alison MR. *The biology of epithelial cell populations* (Volumes I and II). Oxford: Clarendon Press, 1984.
3 Appleton DR, Sunter JP, Watson AJ. *Cell proliferation in the gastrointestinal tract.* Bath: The Pitman Press, 1980.
4 Potten CS, Loeffler M. Stem cells: attributes, cycles, spirals, pitfalls and uncertainties. Lessons for and from the crypt. *Development* 1990; **110:** 1001–20.
5 Schmidt GH, Winton DJ, Ponder BAJ. Development of the pattern of cell renewal in the crypt-villus unit of chimaeric mouse small intestine. *Development* 1988; **103:** 785–90.
6 Cheng H, Leblond CP. Origin, differentiation and renewal of the four main epithelial cell types in the mouse small intestine. *Am J Anat* 1974; **141:** 537–63.
7 Hauft SM, Kin SH, Schmidt GH, Pease S, Rees S, Harris S, *et al.* Expression of SV-40 T antigen in the small intestinal epithelium of transgenic mice results in proliferative changes in the crypt and reentry of villus-associated enterocytes into the cell cycle but has no apparent effect on cellular differentiation programs and does not cause neoplastic transformation. *J Cell Biol* 1992; **117:** 825–39.
8 Louvard D, Kedinger M, Hauri HP. The differentiating intestinal epithelial cell: establishment and maintenance of functions through interactions between cellular structures. *Annu Rev Cell Biol* 1992; **8:** 157–95.
9 Walker-Smith JA, Phillips AD, Walford N, Gregory H, Fitzgerald JD, MacCullagh K, *et al.* Intravenous epidermal growth factor/urogastrone increases small intestinal cell proliferation in congenital microvillus atrophy. *Lancet* 1985; ii: 1239–40.
10 Wright NA, Pike C, Elia G. Induction of a novel epidermal growth factor-secreting cell lineage by mucosal ulceration in human gastrointestinal stem cells. *Nature* 1990; **343:** 82–5.
11 Barnard JA, Beauchamp RD, Russel WE, Dubois RN, Coffey RJ. Epidermal growth factor-related peptides and their relevance to gastrointestinal pathophysiology. *Gastroenterology* 1995; **108:** 564–80.

12 Potten CS. The significance of spontaneous and induced apoptosis in the gastrointestinal tract of mice. *Cancer Metastasis Rev* 1992; **11:** 179–95.
13 Maluenda C, Phillips AD, Briddon A, Walker-Smith JA. Quantitative analysis of small intestinal mucosa in cow's milk-sensitive enteropathy. *J Pediatr Gastroenterol Nutr* 1984; **3:** 349–56.
14 Davidson GP, Cutz E, Hamilton JR, Gall DG. Familial enteropathy: a syndrome of protracted diarrhea from birth, failure to thrive, and hypoplastic villus atrophy. *Gastroenterology* 1978; **75:** 783–90.
15 Cutz E, Rhoads JM, Drumm B, Sherman PM, Durie PR, Fostner GG. Microvillus inclusion disease: an inherited defect of brush-border assembly and differentiation. *N Engl J Med* 1989; **320:** 646–51.
16 Trier JS, Browning TD. Epithelial-cell renewal in cultured duodenal biopsies in coeliac disease. *N Engl J Med* 1970; **283:** 1245–50.
17 Wright N, Watson A, Morley A, Appleton D, Marks J. Cell kinetics in flat (avillous) mucosa of the human small intestine. *Gut* 1973; **14:** 701–10.
18 Wright N, Watson A, Morley A, Appleton D, Marks J, Douglas A. The cell cycle time in the flat (avillous) mucosa of the human small intestine. *Gut* 1973; **14:** 603–6.
19 Kosnai I, Kuitunen P, Savilahti E, Rapola J, Kohegyi J. Cell kinetics in the jejunal crypt epithelium in malabsorption syndrome with cow's milk protein intolerance and in coeliac disease of childhood. *Gut* 1980; **21:** 1041–6.
20 Walker-Smith JA, Digeon B, Phillips AD. Evaluation of a casein and a whey hydrolysate for treatment of cow's milk sensitive enteropathy. *Eur J Pediatr* 1989; **149:** 68–71.
21 Meeuwisse GW. Diagnostic criteria in coeliac disease. *Acta Pediatr Scand* 1970; **59:** 461–3.
22 Walker-Smith JA, Guandalini S, Schmitz J, Shmerling DH, Visakorpi JK. Revised criteria for diagnosis of coeliac disease. *Arch Dis Child* 1990; **65:** 909–11.
23 Phillips AD, Thomas AG, Walker-Smith JA. Cryptosporidiosis, chronic diarrhoea and the proximal small intestinal mucosa. *Gut* 1992; **33:** 1057–61.
24 Hill SM, Phillips AD, Walker-Smith JA. Enteropathogenic E coli and life threatening chronic diarrhoea. *Gut* 1991; **32:** 154–8.
25 Gerdes J, Schwab H, Lemke H, Stein H. Production of a mouse monoclonal antibody reactive with a human nuclear antigen associated with cell proliferation. *Int J Cancer* 1983; **31:** 13–20.
26 Schluter C, Duchrow M, Wohlenberg C, Becker MHG, Key G, Flad HD, *et al.* The cell proliferation- associated antigen of antibody Ki-67: a very large, ubiquitous nuclear protein with numerous repeated elements, representing a new kind of cell cycle-maintaining proteins. *J Cell Biol* 1993; **123:** 513–22.
27 Falini B, Flenghi L, Fagiolo M, Stein H, Schwarting R, Riccardi C, *et al.* Evolutionary conservation in various mammalian species of the human proliferation-associated epitope recognised by the Ki-67 monoclonal antibody. *J Histochem Cytochem* 1989; **37:** 1471–8.
28 Kellet M, Potten CS, Rew DA. A comparison of in vivo cell proliferation measurements in the intestine of mouse and man. *Epithelial Cell Biology* 1992; **1:** 147–55.
29 Savidge TC, Walker-Smith JA, Phillips AD. Novel insights into human intestinal epithelial cell proliferation in health and disease using confocal microscopy. *Gut* 1995; **36:** 369–74.
30 Phillips AD, Walker-Smith JA. Role of small bowel biopsy in diagnosis. *Baillieres Clin Pediatr* 1994; **2:** 645–66.
31 Totafurno J, Bjerkes M, Cheng H. Variation in crypt size and its influence on the analysis of epithelial cell proliferation in the intestinal crypt. *Biophys J* 1988; **54:** 845–58.
32 Przemioslo R, Wright NA, Elia G, Ciclitira PJ. Analysis of crypt cell proliferation in coeliac disease using MIB-1 antibody shows an increase in growth fraction. *Gut* 1995; **36:** 22–7.
33 Tannock IF. A comparison of the relative efficiencies of various metaphase arrest agents. *Exp Cell Res* 1967; **47:** 345–56.
34 Shmakov AN, Morey AL, Ferguson DJP, Fleming KA, O'Brien JA, Savidge TC. Conventional patterns of human intestinal proliferation in a severe-combined immunodeficient xenograft model. *Differentiation* 1995; **59:** 321–30.
35 Scott RJ, Hall PA, Haldane JS, van Noorden S, Price Y, Lane DP, *et al.* A comparison of immunohistochemical markers of cell proliferation with experimentally determined growth fraction. *J Pathol* 1991; **165:** 173–8.
36 Marin L, Aperia A, Zetterstom R, Gunoz H, Sokucu S, Saner G, *et al.* Unsuccessful oral rehydration in an infant with enteropathogenic E coli diarrhoea. Studies of fluid and electrolyte homeostasis. *Acta Paediatr Scand* 1985; **74:** 477–9.